DAS coupling noise suppression based on MCA-FK

Yankai Xu[1] Hongduo Zhu[1] Siyuan Cao[2] Siyuan Chen[2] Jiawei Li[1] Hongwei Liu[1]

1 College of Information Science and Engineering, China University of Petroleum-Beijing, Beijing, China

2 College of Geophysics, China University of Petroleum-Beijing, Beijing, China

Abstract: In recent years, distributed fiber acoustic sensor (DAS) technology has been applied for high-precision acquisition of vertical seismic profile (VSP) data, which has the advantages of high-density acquisition, low cost, safety and coordination. However, coupling noise with characteristics similar to that of the spring is produced and mixed in the VSP data collected by the distributed optical fiber in the well. The energy of the coupling noise tends to be very strong, resulting in the effective VSP data being covered. In this paper, coupling noise is constructed by analyzing its morphological characteristics. The dictionaries of coupling noise and clean VSP data are constructed respectively using their different characteristics, and the morphological component analysis (MCA) algorithm is proposed to separate them. The alternating direction multiplier method (ADMM) is used to solve the objective function, for which both L1 and L2 norm regularizations are adopted in the MCA algorithm. However, the performance of the algorithm heavily relies on the coefficient selection of the threshold, which can lead to noise residue in the denoised VSP data and effective signal attenuation due to the inappropriate selection of the threshold. Therefore, the frequency-wavenumber (FK) transform is further used to extract VSP data from the separated coupling noise. The proposed MCA and FK transform (MCA-FK) algorithm is applied to the field data and has achieved good results.

Keywords: Coupling noise suppression; DAS; MCA-FK; ADMM

1. introduction

With the rapid development of distributed fiber acoustic sensor (DAS) technology, it is used in various fields of industry. DAS technology is used for downhole high-precision seismic data acquisition and the vertical seismic profile (VSP) data imaging by having the advantages of low cost, corrosion resistance, easy data transmission, high precision and high sensitivity. The principle is to transform the optical signal into seismic signal by the change of optical path in the optical fiber caused by the earthquake.

As a new type of seismic detection technology, DAS technology was first proposed at the 2011 SEG annual meeting. Mestayer et al. (2011) analyzed the data collected by DAS and that by traditional geophones and concluded that the seismic data and resolution generated by the two means are basically the same. Daley et al. (2013) and Mateeva et al. (2014) introduced the principle of the data acquisition with DAS technology in seismic exploration. They also processed and interpreted the field data and pointed out many advantages and future challenges of DAS technology.

However, as a new development technology, the coupling noise similar to the spring is produced because the optical fiber cable can’t be better coupled with the well resulting in coherent cable beat when the VSP data is collected by the distributed optical fiber in the well. YU et al. (2016) analyzed and fitted parameters of the cable ringing noise, including with the first breaking time, amplitude, period and average wavelet. Chen et al. (2018) proposed DCT dictionary and wavelet dictionary denoising based on sparse optimization, and removed coupling noise by different characteristics of coupling noise and effective signal. However, coupling noise residue still present especially near the first arrival wave via the method because coupling noise will be attenuated with the increase of depth. Hou et al. (2021) improved chen's method via adaptively calculating the length of the coupling noise contained in each trace of the VSP data, so the coupling noise near the first arrival wave is better suppressed. Gu et al. (2021) removed the coupling noise by forward modeling for the attenuation curve of the coupling noise. Lv et al. (2022) optimized the function for obtaining the coupling noise's parameters of amplitude, phase and frequency and then removing it. Shao et al. (2022) developed a time–frequency analysis method based on low-rank and sparse matrix decomposition and data position points distribution maps to separate signals from the coupling noise. Based on deep learning, Dong et al. (2022) and Zhong et al. (2022) constructed the high-precision deep learning denoising network which can effectively suppress the noise in VSP data and improved the signal-to-noise ratio of denoising results.

Inspired by Chen et al. (2018), we proposed MCA and FK transform (MCA-FK) algorithm to better attenuate the coupling noise. In this paper, the model of coupling noise is firstly constructed based on analyzing its frequency component and the more suitable dictionaries of coupling noise and clean VSP data are constructed respectively. Then the alternating direction multiplier method (ADMM) to solve the objective function of which L1 and L2 norm regularizations are adopted in the MCA algorithm. In addition, the frequency-wavenumber (FK) transform is further used to extract the useful signal which is remained in the separated coupling noise because of inappropriate selection of the threshold in MAC algorithm. Finally, the proposed MCA-FK algorithm is applied to the field data and has achieved good results.

2. Principle

2.1 Analysis of coupling noise and VSP data

The noisy VSP data y contains clean VSP data s_0、coupling noise s_1 and random noise n :

$$\mathrm{y} = \mathrm{s}_0 + \mathrm{s}_1 + \mathrm{n} \tag{1}$$

The formation of coupling noise is mainly due to the fact that the optical fiber cable fails to couple well with the wellbore. The vibration caused by the earthquake makes the unfixed optical fiber cable beat back and forth, forming a noise with strong energy similar to the sawtooth waveform. When the maximum distance of the unfixed optical fiber cable is A, and the vibrational velocity of the optical fiber cable is V, the back and forth beats process of the cable can be described with the relationship between the distance d of the acoustic sensor system recording the vibration and the travel time t (Gu et al. 2021). It can be represented as:

$$\mathrm{d(t)} = \begin{cases} \left(\mathrm{t\ mod}\left(\frac{2A}{V}\right)\right)\mathrm{V} & 0 \le \mathrm{t\ mod}\left(\frac{2A}{V}\right) \le \frac{A}{V} \\ \mathrm{A} - \left(\mathrm{t\ mod}\left(\frac{2A}{V}\right)\right)\mathrm{V} & \frac{A}{V} \le \mathrm{t\ mod}\left(\frac{2A}{V}\right) \le \frac{2A}{V} \end{cases} \tag{2}$$

where a mod b means the remainder of a divided by b.

The function of the reflection coefficient r(t) of the sensor system recorded with the travel time t is equal to that of d(t), and its waveform is shown in Fig.1a. The coupling noise s_1(t) can be expressed as the convolution of the reflection coefficient r(t) and Ricker wavelet w(t):

$$s_1(t) = w(t) * r(t) \tag{3}$$

The waveform characteristics of s_1(t) (Fig.1b) are completely consistent with those of the coupling noise in the field data (Fig.1c).

To verify the correctness of the coupling noise model, time-frequency spectrum analysis was performed on some traces of the coupling noise model and the field data that is interfered by the coupling noise. Fig.2a and 2b show two traces from Fig.1b, and Fig.2c shows one trace from Fig.1c. Fig.2a and 2b exhibit periodic oscillating waveforms because the function of reflection coefficient r(t) is periodic. Fig.2d and 2e represent the frequency spectra of Fig.2a and 2b, respectively. Since the frequency of the reflection coefficient is 50Hz (Fig.1a), there is a fundamental frequency of 50Hz and a second harmonic frequency of 100Hz in both Fig.2d and 2e. Fig.2f displays the frequency spectrum of Fig.2c, and its peaks at 15Hz and 30Hz indicate that the coupling noise in the field data also contains harmonic components.

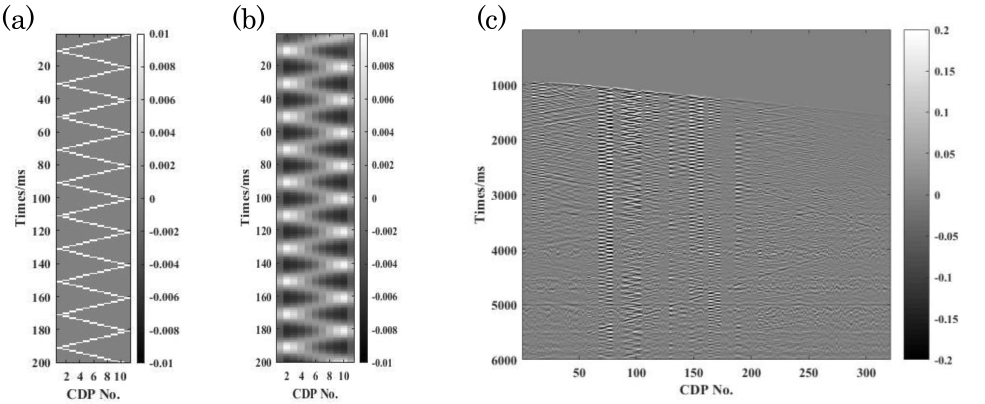

Fig.1 Coupling noise model. a) relationship between the reflection coefficient of sensor system record and the travel time; b) model of coupling noise; c) field data

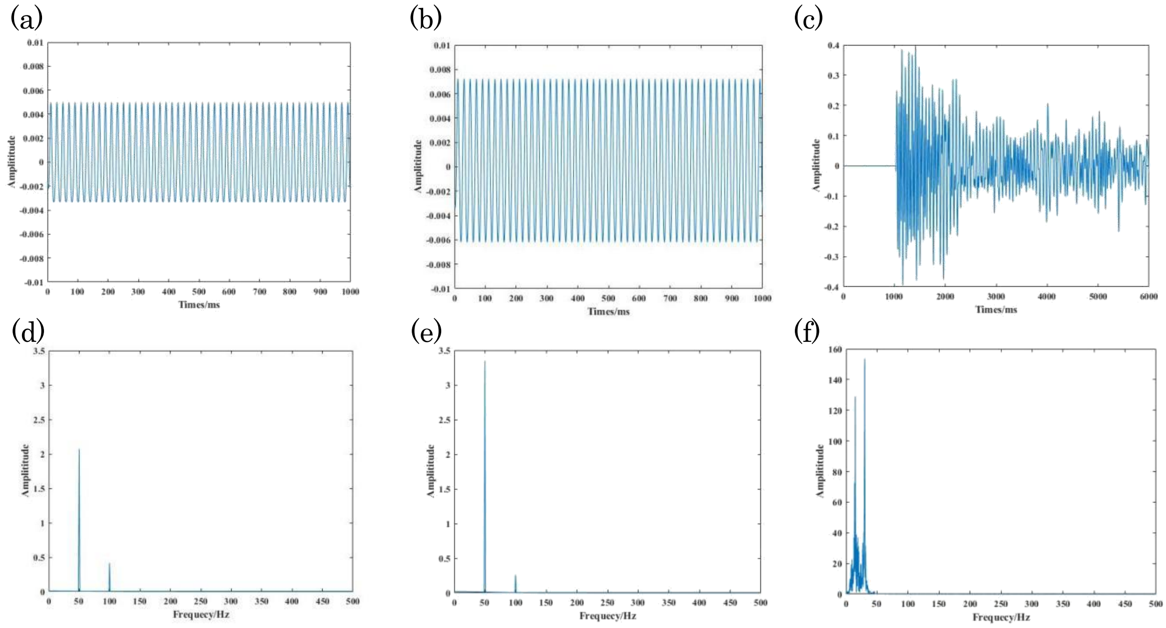

Fig.2 Time-frequency domain analysis of coupling noise. a) the first trace of Fig.1b; b) the third trace of Fig.1b; c) the74th trace of Fig.1c; d) the spectrum of a); e) the spectrum of b); f) the spectrum of c).

The clean VSP data (Fig.3a) is the convolution of Ricker wavelet and the formation reflection coefficient. The waveform of the 20th trace (Fig.3b) is composed of Ricker wavelets and it has continuous frequency distribution (Fig.3c) because the formation reflection coefficient is aperiodic. Therefore, the VSP data can be formed by superposition of Ricker wavelet.

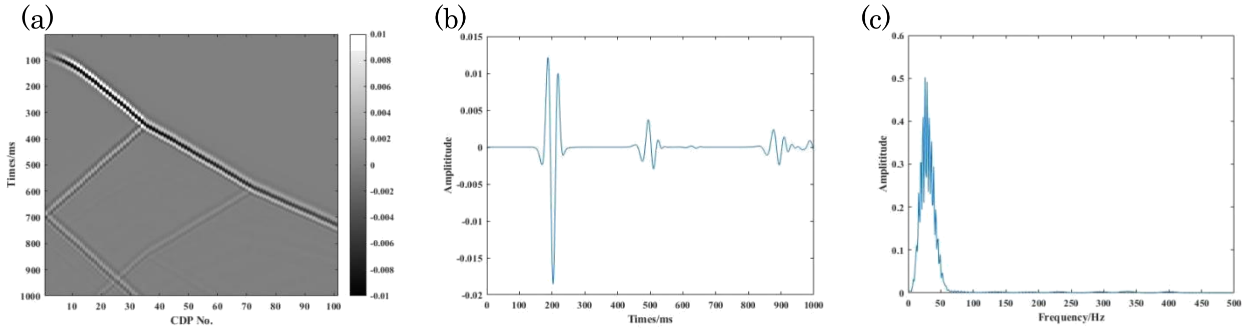

Fig.3 Time-frequency domain analysis of VSP model. a) VSP model; b) the 20th trace of a); c) the spectrum of b)

2.2 Theory of MCA-FK

2.2.1 MCA

As long as the signal is compressible or sparse in a transform domain, the transformed high-dimensional signal can be projected onto a low-dimensional space with an observation matrix that is not related to the transform basis base on the theory of compressed sensing (Pilikos 2020). Morphological component analysis (MCA) is a compressed sensing framework (Starck et al. 2005; Chen et al. 2018). Several signals can be separated by MCA method because they have their sparse morphological characteristics of different signal components in different transform domains. They can be reconstructed respectively from their small projections with high probability by solving an optimization problem.

According to the MCA theory, we assume that s_0 can be expressed by dictionary A_0 and sparse matrix x_0, s_1 can be expressed by dictionary A_1 and sparse matrix x_1, whereas A_0 cannot express s_1 and A_1 cannot express s_0, so the expression (1) can be described as (Chen et al. 2018):

$$y = A_0 x_0 + A_1 x_1 + n \tag{4}$$

The x_0 and x_1 matrices should be sparse enough, so we rewrite (4) as the following minimization problem with L0 norm regularization:

$$\arg\min_{x_1, x_0} \|x_0\|_0 + \|x_1\|_0 \quad \text{s.t.} \quad \|Y - A_0 x_0 - A_1 x_1\|_2^2 \le \delta \tag{5}$$

The solution of L0 norm is an np-hard problem which can be replaced as L1 norm, so the minimization problem (5) is rewritten as:

$$\arg\min_{x_1, x_0} \|x_0\|_1 + \|x_1\|_1 \quad \text{s.t.} \quad \|Y - A_0 x_0 - A_1 x_1\|_2^2 \le \delta \tag{6}$$

2.2.2 Dictionary

The selection of dictionaries A_0 and A_1 is important for separating clean VSP data and the coupling noise. The selection of dictionaries A_0 and A_1 is important for separating coupling noise and clean VSP data. Dictionaries A_0 and A_1 are respectively composed with Ricker and sine wavelets with different frequencies and different phases based on the analysis of clean VSP data and coupling noise in section 2.1.

The dictionary A_0 is composed of Ricker wavelets with different phases (Fig.4a). The frequency of the Ricker wavelet is determined by the wavelet frequency in the clean VSP data. For example, the frequency of selected Ricker wavelet is 30Hz for the dictionary A_0 of the VSP data in Fig.3. The phase of the Ricker wavelet for each trace is different in the dictionary A_0. The phase of Ricker wavelet at the 100th and 900th trace is shown in Fig.4b and Fig.4c, respectively. The waveform does not change, and the phase moves from left to right.

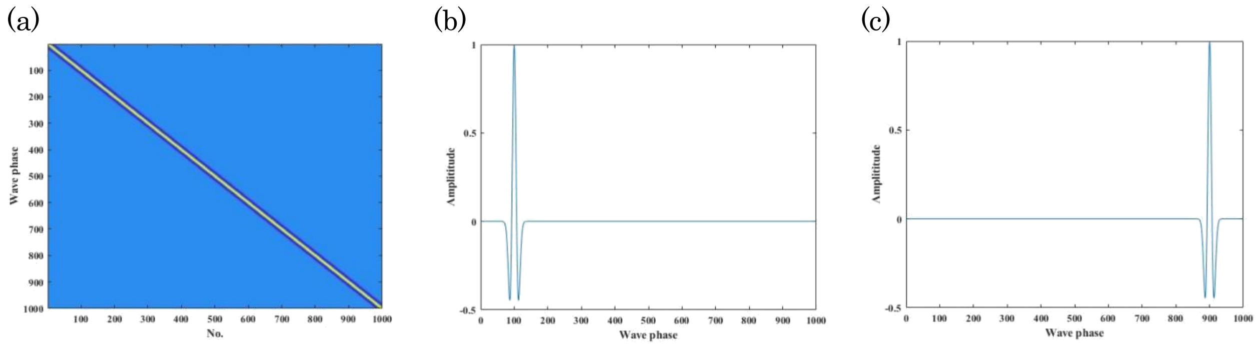

Fig.4 The demonstration of dictionary A_0. a) dictionary A_0. b) the 100th trace of a); c) the 900th trace of a).

The dictionary A_1 is composed of two parts which is constructed by the first and second harmonics of the coupling noise, respectively. For example, the first 1000 traces are 50Hz sinusoidal signals (Fig.5b), and the last 1000 traces are 1000Hz sinusoidal signals (Fig.5c) in the dictionary A_1 (Fig.5a) of the coupling noise model (Fig.1b). In addition, the phase of the two independent parts also moves from left to right in their dictionaries, respectively.

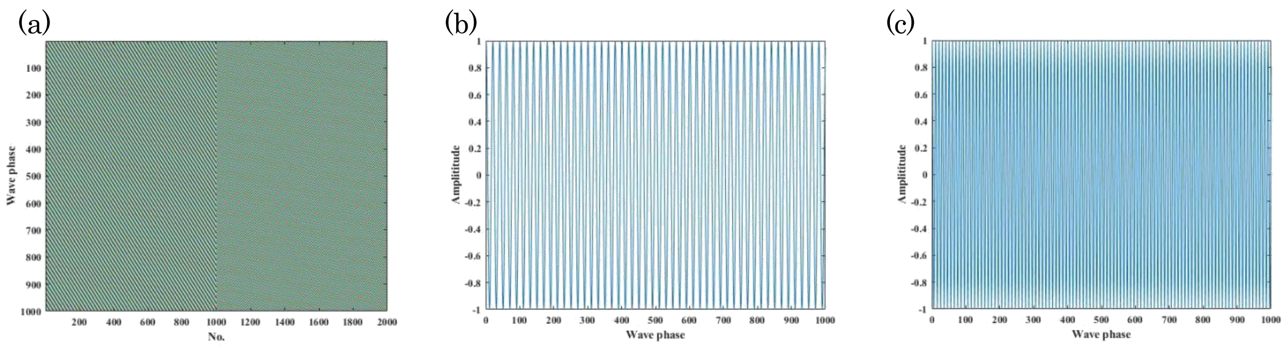

Fig.5 The demonstration of dictionary A_1. a) dictionary A_1. b) the 100th trace of a); c) the 1200th trace of a).

2.2.3 ADMM iterative solution

The ADMM algorithm (Shi et al. 2014; Aghamiry et al. 2020) is used to solve the above problem (6). The ADMM algorithm provides a framework for solving optimization problems with linear equality constraints. It is convenient for us to use the augmented Lagrangian algorithm (ALM) to decompose the original optimization problem into several relatively good sub-optimization problems for iterative solution. We introduce z_1、z_0, and let $x_1 = z_1$、$x_0 = z_0$. We also refer to the update compensation intermediate parameters u_1、u_0, and the iteration step ρ_1、ρ_0. The Lagrange function of the problem is written as:

$$I(x_0, x_1, z_0, z_1, u_0, u_1) = \underset{x_0, x_1, z_0, z_1, u_0, u_1}{\arg\min} \frac{1}{2}\|Y - A_0x_0 - A_1x_1\|_2^2 + \lambda_0\|z_0\|_1 + \lambda_1\|z_1\|_1$$

$$+\frac{\rho_0}{2}\|x_0 - z_0 + u_0\|_2^2 + \frac{\rho_1}{2}\|x_1 - z_1 + u_1\|_2^2 \tag{7}$$

The iterative framework of ADMM algorithm is used to solve the problem (7). In the iterative process, only a single variable is iterated at each step, and other variables are calculated as known variables. For the update iteration of each parameter, only the part containing iterative parameters needs to be considered, so the optimization problem of each parameter is as follows (Shi et al. 2014):

$$P_1(x_0) = \arg\min_{x_0} \frac{1}{2}\|Y - A_0x_0 - A_1x_1\|_2^2 + \frac{\rho_0}{2}\|x_0 - z_0 + u_0\|_2^2 \tag{8}$$

$$P_2(x_1) = \arg\min_{x_1} \frac{1}{2}\|Y - A_0x_0 - A_1x_1\|_2^2 + \frac{\rho_1}{2}\|x_1 - z_1 + u_1\|_2^2 \tag{9}$$

$$P_3(z_0) = \arg\min_{z_0} \lambda_0\|z_0\|_1 + \frac{\rho_0}{2}\|x_0 - z_0 + u_0\|_2^2 \tag{10}$$

$$P_4(z_1) = \arg\min_{z_1} \lambda_1\|z_1\|_1 + \frac{\rho_1}{2}\|x_1 - z_1 + u_1\|_2^2 \tag{11}$$

$$P_5(u_0) = \arg\min_{u_0} \frac{\rho_0}{2}\|x_0 - z_0 + u_0\|_2^2 \tag{12}$$

$$P_6(u_1) = \arg\min_{u_1} \frac{\rho_1}{2}\|x_1 - z_1 + u_1\|_2^2 \tag{13}$$

The parameters of each step are solved to obtain the updated iterative algorithm. The latest parameters obtained by each update iteration will enter the algorithm of the next parameter iteration.

$$x_0^{(k+1)} = (A_0^TA_0 + \rho_0 I)^{-1}[\rho_0(z_0^{(k)} - u_0^{(k)}) + A_0^T(Y - A_1^{(k)}X_1^{(k)})] \tag{14}$$

$$x_1^{(k+1)} = (A_1^TA_1 + \rho_1 I)^{-1}[\rho_1(z_1^{(k)} - u_1^{(k)}) + A_1^T(Y - A_0^{(k)}X_0^{(k+1)})] \tag{15}$$

$$z_0^{(k+1)} = T_{\lambda_0/\rho_0}(x_0^{(k+1)} + u_0^{(k)}) \tag{16}$$

$$z_1^{(k+1)} = T_{\lambda_1/\rho_1}(x_1^{(k+1)} + u_1^{(k)}) \tag{17}$$

$$u_0^{(k+1)} = u_0^{(k)} + x_0^{(k+1)} - z_0^{(k+1)} \tag{18}$$

$$u_1^{(k+1)} = u_1^{(k)} + x_1^{(k+1)} - z_1^{(k+1)} \tag{19}$$

where k represents the number of iterations and $T_{\lambda/\rho}(S)$ is soft-thresholding operator (Liu et al. 2016):

$$T_{\lambda/\rho}(S) = \mathrm{sign}(S) \cdot \max(|S| - \lambda/\rho, 0) \tag{20}$$

Among them, ρ_0=ρ_1=1, by adjusting the size of λ_0 and λ_1, the effective signal and coupling noise are separated.

2.2.4 FK transform

Because the performance of MCA method to suppress coupling noise relies heavily on the coefficient selection of the threshold function, the inappropriate coefficient often leads to a certain amount of noise residues in the denoised VSP data.

The FK filtering (Draganov et al. 2009) method is based on the principle of two-dimensional Fourier transform. It can convert the VSP data from the function f (t, x) represented by the reflection time t and the trace position x into a function F (f, k) represented by frequency and spatial wave number k, that is:

$$F(f,k) = \int_{-\infty}^{+\infty}\int_{-\infty}^{+\infty} f(t,x)e^{-2\pi i(ft+kx)}dt\,dx \tag{21}$$

The FK diagram shown in Fig.6a has zones 1-3 which are regarded as a high-speed, medium-speed and low-speed zone, respectively. Since the apparent velocities of the effective signal and coupling noise in the noisy VSP data are different, they will be centered in different regions in FK domain. The FK diagram of VSP data is shown in Fig.6b. Because the cable beats fast, the coupling noise is distributed in the high-speed area of the first zone, and the effective VSP signal is distributed in the medium-speed area of the second zone. According to this feature, a filter can be designed in the FK domain to separate the effective signal in the separated coupling noise after using MCA method. The use of FK transform will reduce the impact of the threshold function and improve the signal-to-noise ratio.

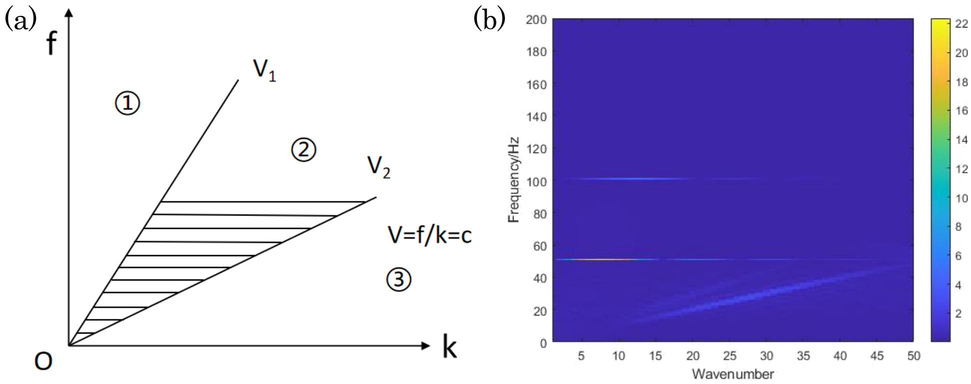

Fig.6 FK spectrum. a) FK spectrum; b) FK spectrum of noisy VSP data.

3. Examples

3.1 Synthetic data

The synthetic coupling noise and clean VSP data model are superimposed, and random noise is added to synthesize the noisy VSP model (Fig.7a). The separated results using MCA and MCA-FK algorithms, respectively. The dictionaries A_0 and A_1 are constructed based on the principle in section 2.2.2. λ_0 is 5×10^{-4} and λ_1 is 5×10^{-6}. Most of the coupling noise and random noise (Fig.7c) can be separated from noisy data with MCA algorithm, however there are still some residual signal in separated noise. Meanwhile there are some noise in the separated signal (Fig.7b). Compared with those of MCA, the separated noise

(Fig.7d) and the effective signal (Fig.7e) via MCA-FK algorithm are separated more effective. Fig.8a is the 31st trace of noisy VSP model (Fig.7a) and the subgraphs in Fig.8 correspond to those of Fig.7. As can be seen from figures 7 and 8, the effective signal is basically undisturbed and the coupled noise and random noise are successfully suppressed via MCA-FK algorithm.

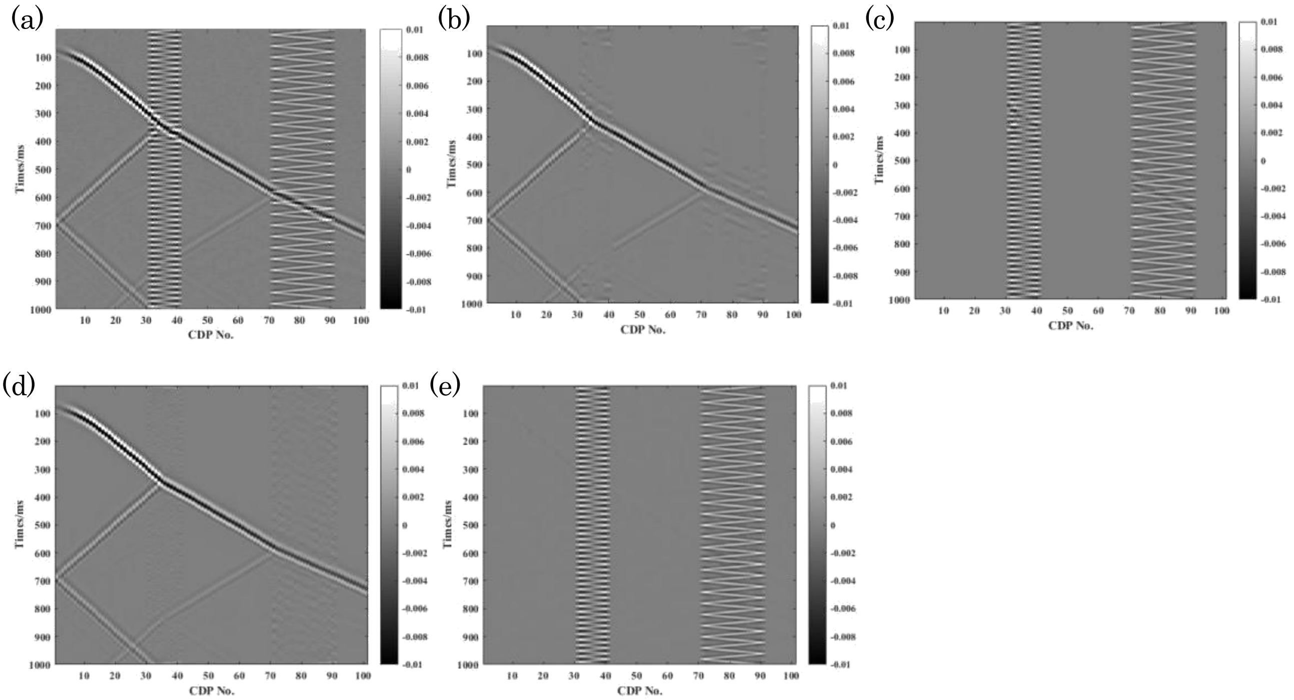

Fig.7 Denoising of noisy VSP model. a) noisy VSP model; b) denoised effective signal via MCA; c) separated noise via MCA; d) separated effective signal via MCA-FK; e) separated noise via MCA-FK;

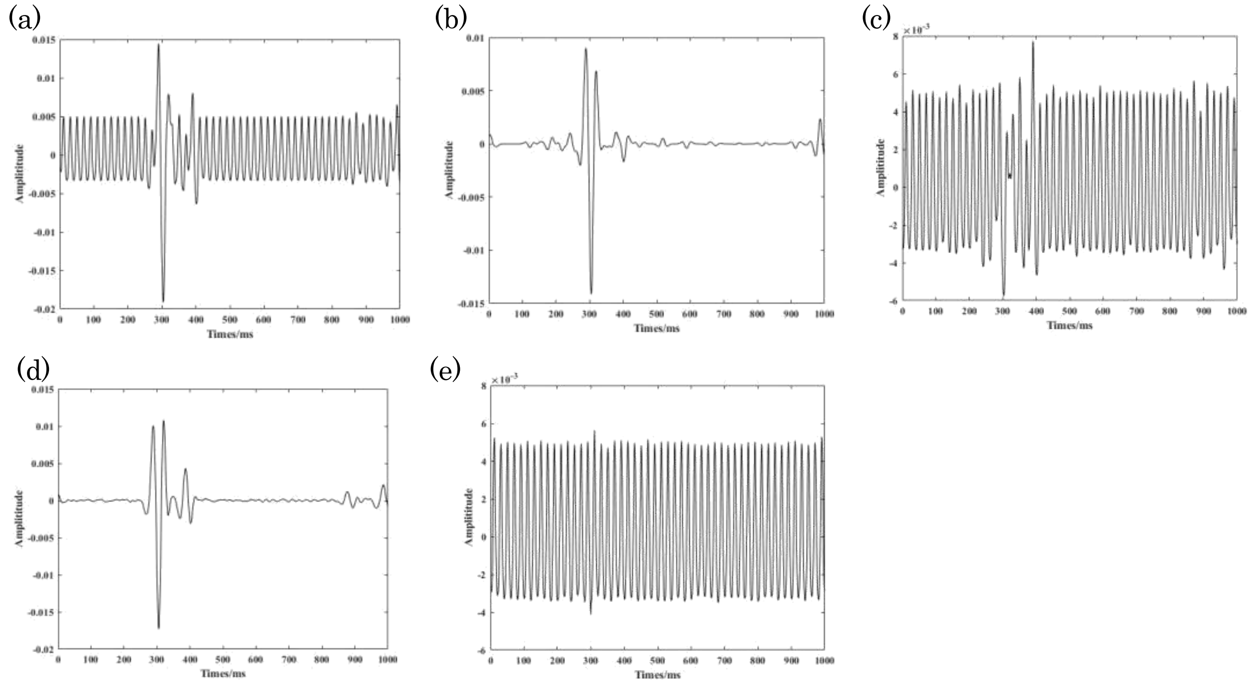

Fig.8 Demonstration of a trace in Fig.7. a) the 31th trace of Fig.7a); b) denoised effective signal via MCA; c) separated noise via MCA; d) separated effective signal via MCA-FK; e) separated noise via MCA-FK;

3.2 Field data

To further demonstrate the performance of MCA-FK in practice, we choose the field VSP data (Fig.9a) from eastern China. The field data is much more complex than the VSP model. The field VSP signal is seriously disturbed by the coupling noise and random noise.

The noisy VSP data is processed via MCA and MCA-FK algorithms, respectively. In these processing, the length of the processing window is 200. For the dictionary A_0 shown in Fig.9b of the effective signal, the appropriate Ricker wavelet is selected by analyzing the spectrum of some traces undisturbed by the coupling noise in the field VSP data. As shown in Fig.9c, the trace reconstructed (green) using the Ricker wavelet dictionary is almost identical with the original signal(black).

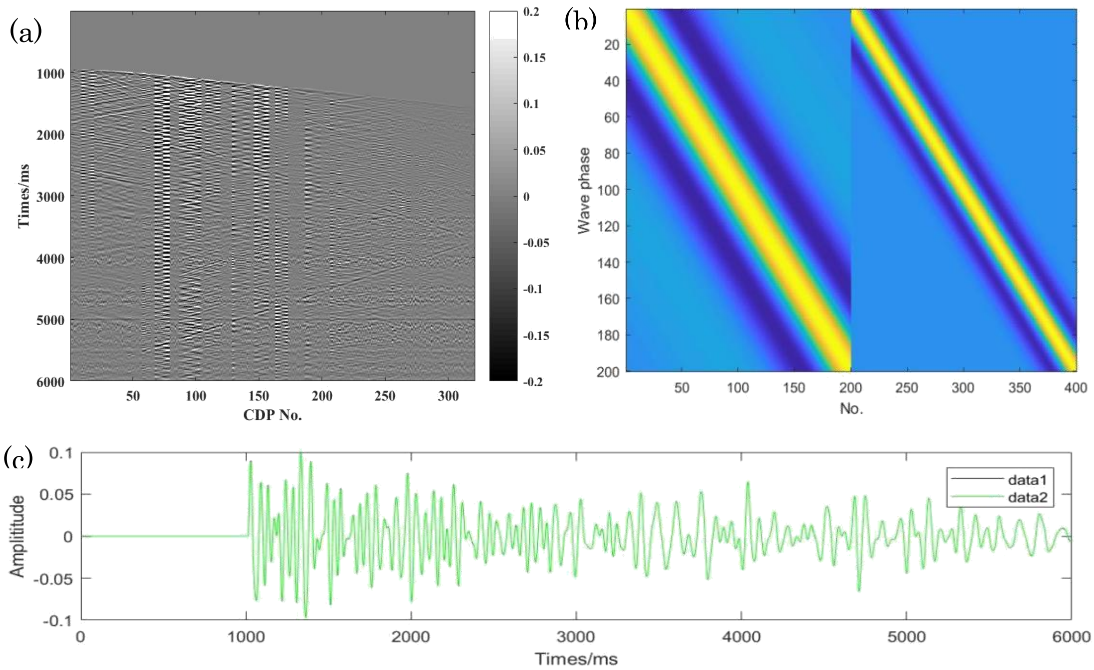

Fig.9 Demonstration of data reconstructed with dictionary A0. a) field data; b) dictionary A0; c) original trace undisturbed by coupling noise (black) and its reconstruction (green).

The spectrum analysis of each part of the coupling noise interference is carried out to determine the frequency characteristics and number N of the coupling noise, and spliced into an over-complete dictionary A_1, The row size of the dictionary A_1 is 200 and the column size is 200*N(Fig.10e). The separated effective signal and the coupling noise via MCA are shown in Fig.10a and b, respectively. It can be clearly observed that the part of the original signal covered by the coupling noise is missing, and the missing part appears in the extracted coupling noise. Because the coupling noise presents a regular signal, and the FK transform has a strong suppression effect on such signals, the VSP signal contained in the coupling noise can be extracted to reconstruct the effective signal (Fig.10c) by the MCA-FK algorithm. At the same time, the coupled noise and random noise (Fig.10d) are more successfully suppressed. In addition, the field data also contains some similar transverse waves left by VSP data preprocessing, which is not processed in this paper.

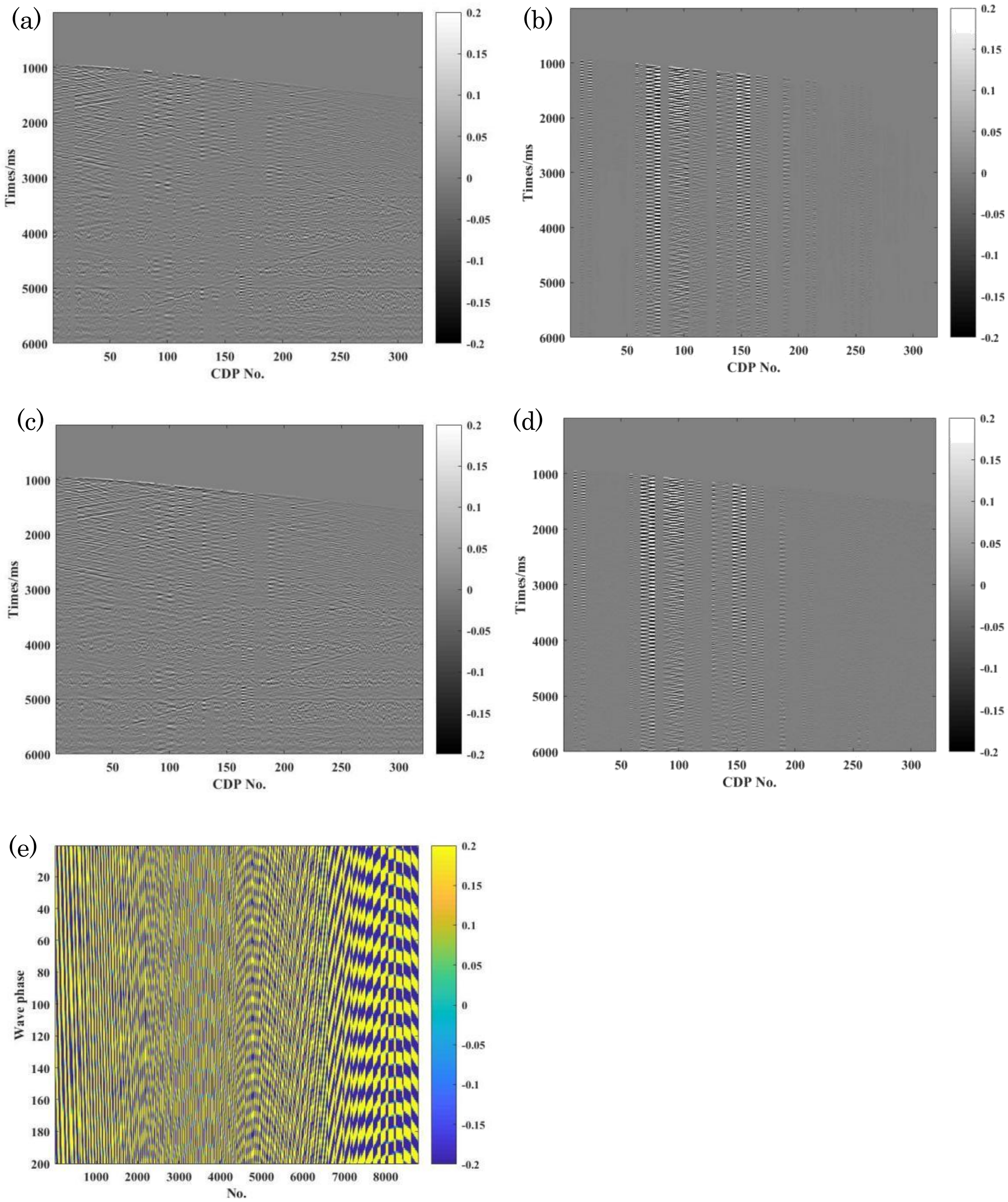

Fig.10 Demonstration of denoised results for field data in Fig.9a. a) the separated VSP signal via MCA; b) the separated noise via MCA; c) the separated VSP signal by MCA-FK. d) the separated noise by MCA-FK; e) dictionary A1.

4. Conclusion

In this paper, the algorithm of DAS coupling noise suppression based on MCA and FK transform is proposed. Firstly, through the different characteristics of effective signal and coupling noise, the high-dimensional space dictionaries are constructed for effective signal and coupling noise, respectively.

Secondly, the noisy VSP data can be separated into effective signal, coupling noise and random noise through MCA algorithm which is competed by solving the objective function including L1 and L2 norm regularizations with ADMM. Finally, FK transform is used to extract the residue effective signal in the separated coupling noise. Synthetic and field data examples demonstrate that the proposed algorithm can successfully suppress the coupling noise and random noise for the noisy VSP data.

COF statement

On behalf of all authors, the corresponding author states that there is no conflict of interest.

REFERENCES

Aghamiry H S, Gholami A, Operto S (2020) Multiparameter wavefield reconstruction inversion for wave speed and attenuation with bound constraints and total variation regularization. Geophysics 85 (4):R381–R396.

Chen J, Chen W, Wang X, Zhou Y, Zhang G (2018) DAS coupling noise suppression using wavelet and DCT dictionary based on sparse optimization. SEG Technical Program Expanded Abstracts 2018.

Chen J, Ning J, Chen W, Wang X, Zhang G (2018) Distributed acoustic sensing coupling noise removal based on sparse optimization. Interpretation 7(2):1-58.

Daley T M, Freifeld B M, Ajo-Franklin J, Dou S, Pevzner R, Shulakova V, Miller DE, Goetz J, Henninges J (2013) Field testing of fiber-optic distributed acoustic sensing (DAS) for subsurface seismic monitoring. The Leading Edge 32(6): 936-942.

Dong X, Li Y, Zhong T, Wu N, Wang H (2022) Random and coherent noise suppression in DAS-VSP data by using a supervised deep learning method. IEEE Geoscience and Remote Sensing Letters 19:1-5.

Draganov D, Campman X, Thorbecke J, Verdel A, Wapenaar K (2009) Reflection images from ambient seismic noise. Geophysics 74(5): A63-67.

Gu Y, Mu F (2021) Suppression of the spring wave in VSP data acquired by the DAS system based on a forward modeling method. Chinese Journal of Engineering Geophysics 18(4):409-415.

Hou Q, Liu D, Wang X, Chen W (2021) Adaptive DAS coupling noise suppression based on local MCA. First International Meeting for Applied Geoscience & Energy.

Liu Y, Zhan Z, Cai J, Di G, Zhong C, Qu X (2016) Projected iterative soft-thresholding algorithm for tight frames in compressed sensing magnetic resonance imaging. IEEE Transactions on Medical Imaging 35(9): 2130

-2140.

Lv G, Mu F, Liu X, Liu X, Shan Y (2022) Analysis and suppression of interference wave of DAS system in borehole. Geophysical Prospecting for Petroleum. 61(1):85-92.

Mateeva A, Lopez J, Potters H, Mestayer J, Cox B, Kiyashchenko D, Wills P, Grandi S, Hornman K, Kuvshinov B (2014) Distributed acoustic sensing for reservoir monitoring with vertical seismic profiling. Geophysical Prospecting 62(4), 679-692.

Mestayer J, Cox B, Wills P, Kiyashchenko D, Lewis A B (2011) Field Trials of Distributed Acoustic Sensing for Geophysical Monitoring. Seg Technical Program Expanded.

Pilikos G (2020) The relevance vector machine for VSP Bayesian compressive sensing. Geophysics 2020; 85 (4): WA279–WA292.

Shao D, Li T, Han L, Li Y (2022) Noise suppression of distributed acoustic sensing vertical seismic profile data based on time–frequency analysis. Acta Geophysica 70:1539–1549.

Shi W, Ling Q, Yuan K, Wu G, Yin W. (2014) On the Linear Convergence of the ADMM in Decentralized Consensus Optimization. IEEE Transactions on Signal Processing.62(7):1750-1761.

Starck J L, Elad M, Donoho D L (2005) Image decomposition via the combination of sparse representations and a variational approach. IEEE Transactions on Image Processing. 14(10):1570–1582.

Yu G, Greer J, Zhang Q, Chen Y, Liu C, Wang Y, Li Y, Wang X (2016) Walkaway VSP using multimode optical fibers in a hybrid wireline. The Leading Edge 35(7): 615-619.

Zhong T, Cheng M, Lu S, Dong X, Li Y (2022) A deep-learning-based background noise suppression Method for DAS-VSP Records. IEEE Geoscience and Remote Sensing Letters 19:1-5.